PCCP

PAPER

View Article Online
View Journal | View Issue

Cite this: *Phys. Chem. Chem. Phys.*, 2015, **17**, 16405

Characterization of an abnormal photoluminescence behavior upon crystal-phase transition of perovskite $CH_3NH_3PbI_3$†

Weiguang Kong,[a] Zhenyu Ye,[a] Zhen Qi,[b] Bingpo Zhang,[a] Miao Wang,[a] Arash Rahimi-Iman[c] and Huizhen Wu*[a]

Received 5th May 2015,
Accepted 27th May 2015

DOI: 10.1039/c5cp02605a

www.rsc.org/pccp

Solution-processed hybrid perovskite of $CH_3NH_3PbI_3$ ($MAPbI_3$) exhibits an abnormal luminescence behavior at around the tetragonal–orthorhombic phase transition temperature. The combination of time resolved photoluminescence (PL), variable excitation power PL, and variable-temperature X-ray diffraction (XRD) allows us to clearly interpret the abnormal luminescence features in the phase transition region of $MAPbI_3$. Both PL and XRD results unambiguously prove the coexistence of the tetragonal and orthorhombic phases of $MAPbI_3$ in the temperature range of 150 to 130 K. The two luminescence features observed in the orthorhombic phase at $T < 130$ K originate from free excitons and donor–acceptor-pair (DAP) transitions, respectively. The comprehensive understanding of optical properties upon phase transition in $MAPbI_3$ will benefit the development of new optoelectronic devices.

1. Introduction

Novel light-harvesting materials for mesoscopic solar cells such as $CH_3NH_3PbX_3$ (X: Cl, Br, I) have attracted much attention, following the pioneering work on organic–inorganic hybrid perovskites.[1–6] Particularly, a breakthrough in the methylammonium (CH_3NH_3: MA) lead iodide (hereafter denoted as $MAPbI_3$) perovskite was achieved recently, when the energy conversion efficiency of the hybrid perovskite photovoltaic devices was found to reach up to 19.3%.[1] Further studies suggest that $MAPbI_3$ crystals can become even promising for lasing applications.[7–10] According to previous reports,[8,11] tetragonal $MAPbI_3$ exhibits a broad PL band around its band-gap energy of $\sim$1.6 eV. As temperature (T) decreases, tetragonal $MAPbI_3$ transforms into an orthorhombic phase along with an abnormal emission blue-shift. Such orthorhombic $MAPbI_3$ possesses two emission features. Wehrenfennig *et al.*[12] and Wu *et al.*[13] assigned the two emission features to the phase coexistence of orthorhombic and tetragonal phases. However, Fang *et al.*[14] and Xing *et al.*[7] attributed the two features to bound-exciton and free-exciton emissions. No consensus has been reached because of insufficient experimental evidence, especially concerning the underlying physical mechanisms in the phase transition T region. Although the symmetry and electronic structures of $MAPbI_3$ crystals have been widely studied,[15–19] these results could hardly be used to interpret the optical properties of the orthorhombic $MAPbI_3$ because of little consideration of the impact of crystal defects involved. Since the optical properties of a semiconductor material are related to both intrinsic and extrinsic properties, PL spectroscopy is a highly sensitive and useful tool to assess both the intrinsic, *e.g.*, band structure, excitons, and defects, and extrinsic features, such as impurities. Indeed, a comprehensive understanding of the optical properties of the orthorhombic $MAPbI_3$ is required in order to expand the application fields of $MAPbI_3$ and to develop new optoelectronic devices based on this material system.[14]

In this work, time resolved PL (TRPL) and variable-excitation-power PL characterizations are performed to study the luminescence features of $MAPbI_3$ in different T regions. Moreover, the crystalline phase structures of the $MAPbI_3$ crystal are also characterized by variable-temperature X-ray diffraction (XRD). Our results clarify the origin of the two PL features of orthorhombic $MAPbI_3$. As T is between 150 and 130 K, these two PL features are attributed to the phase coexistence of tetragonal and orthorhombic phases with different band-gap energies. As T falls below 130 K, the two PL features are dominated by the donor–acceptor pair (DAP) recombination. We conclude that the tetragonal–orthorhombic phase transition for the solution-processed $MAPbI_3$ is a gradual process, which is related to the defects in the crystal.

[a] *Department of Physics and State Key Laboratory of Silicon Materials, Zhejiang University, Hangzhou, Zhejiang 310027, P. R. China. E-mail: hzwu@zju.edu.cn*
[b] *State Key Laboratory for Infrared Physics, Shanghai Institute of Technical Physics, Chinese Academy of Sciences, 200083, Shanghai, P. R. China*
[c] *Faculty of physics & Material sciences center, Philipps University Marburg, D-35032 Marburg, Germany*

† Electronic supplementary information (ESI) available: Details of PL and structure properties of $MAPbI_3$ used in this work. See DOI: 10.1039/c5cp02605a

2. Experimental section

2.1 CH_3NH_3I synthesis

CH_3NH_3I was synthesized by reacting 30 mL of methylamine (40% in methanol, TCI) and 32.3 mL of hydroiodic acid (57 wt% in water, Aldrich) in a 250 mL round-bottom flask at 0 °C for 2 h with stirring. The precipitate was recovered by putting the solution on a rotary evaporator and carefully removing the solvents at 50 °C. The yellowish raw product methylammonium iodide (CH_3NH_3I) was washed with diethyl ether by stirring the solution for 30 min, a step that was repeated three times, and finally recrystallized from a mixed solvent of diethyl ether and ethanol. After filtration, the solid was collected and dried at 60 °C in a vacuum oven for 24 h.

2.2 $MAPbI_3$ synthesis

The film of $MAPbI_3$ on a Si substrate was formed by dropping a 40 wt% precursor solution of equimolar CH_3NH_3I and PbI_2 in γ-butyrolactone onto the Si wafer which was first hydrophilic treated by the aqueous solution of H_2O_2 and NH_4OH with a volume ratio of $H_2O_2 : NH_4OH : H_2O = 1:1:5$ for 30 min. The film formation was realized by spin-coating at 1500 rpm for 30 s, and then 2500 rpm for 40 min in air. The film coated on the Si wafer led to the change in color upon drying at room temperature, indicating the formation of $MAPbI_3$ in the solid state. The $MAPbI_3$ film was annealed in air for 15 min at 100 °C.

2.3 Characterization

The $MAPbI_3$ film was characterized by X-ray diffraction (XRD) on a PANalytical X-ray diffractometer (Model EMPYREAN) with a monochromatic Cu $K_{\alpha 1}$ radiation. The lattice parameters were precisely determined using Si powders as the internal standard reference material. Steady-state and time-resolved PL spectra were measured using an Edinburgh FLS920 spectroscopy system, using laser excitation at 405 nm. Scanning electron microscopy (SEM) characterization was carried out using a Hitachi S4800 operating at an acceleration voltage of 5 kV.

3. Results and discussion

It is known that surface morphology influences the luminescence features and dynamics of crystal materials. Proper control of the crystalline shape and size could be essential for random lasers.[20,21] Fig. 1 shows the top view SEM of the as-prepared $MAPbI_3$ film with distinct crystal grains. It is seen that the grain sizes of $MAPbI_3$ are between 100–500 nm, similar to the previously reported one.[22] The SEM confirms that the film is conformal and spatially homogeneous. This helps one to exclude the random signals during the following PL measurements.

Fig. 2(a and b) present the PL spectra acquired for the $MAPbI_3$ perovskite-crystal film at temperatures between 300 K and 10 K in steps of 10 K (a detailed picture of temperature-dependent PL can be found in Fig. S1, ESI†). As shown in Fig. 2(a), the maximum of the PL band (labeled 'Peak_T') in tetragonal $MAPbI_3$, which is due to the near-band-edge (NBE) transition,[8,11,12] locates at 783 nm (1.58 eV) at room temperature.

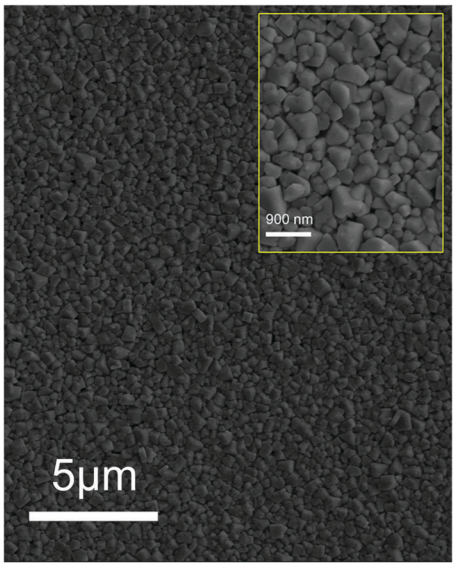

Fig. 1 A top view SEM image showing the surface morphology of the $MAPbI_3$ film. Inset is the enlarged graph for clear observation of the grain size and shape.

NBE here is noted as that the PL of $MAPbI_3$ at variable temperatures could come from the free carrier or free exciton recombination, as Yamada and his coworkers[23,24] found that the exciton binding energy of $MAPbI_3$ could change from ~30 meV at 13 K to 6 meV at 300 K, and the excitons could be dissociated by thermal energy at high temperatures. The location of the PL band agrees well with the latest experimental results, which have proved that the band-gap energy of tetragonal $MAPbI_3$ is ~1.60 eV,[8,11–14,23] rather than 1.5 eV as predicted by theoretical computation. It has been widely accepted in the work related to the area of solar cells.[25–30] Peak_T exhibits a continuous red-shift as T decreases from 300 K to 140 K, which is in contrast to typical semiconductors and may be due to the change in material parameters. With a further decline in T, Peak_T begins to blue shift, leading to the feature at lower temperatures labeled 'Peak_O_{II}' in Fig. 2(b). This fact is in accordance with the observation of variations in the absorption edge of $MAPbI_3$.[12,31] In contrast to the tetragonal phase, the orthorhombic $MAPbI_3$ possesses two PL features, marked Peak_O_I and Peak_O_{II}, as shown in Fig. 2(b). With the decrease in T, Peak_O_I shows a monotonous red shift throughout the whole low temperature range, while Peak_O_{II} initially blue-shifts ($140 > T > 80$ K) and thereafter red-shifts ($T < 80$ K). This complex variation in Peak_O_{II} was also noted in the literature by other groups.[12–14] Here, the strain effect of different substrates on the PL properties of $MAPbI_3$ can be ruled out, since the $MAPbI_3$ grown on different substrates, such as glass,[12,14] quartz,[13] and Si, features similar PL behavior. The intricate variation of the PL spectra observed in the low temperature range is hence attributed to an inherent characteristic of the orthorhombic $MAPbI_3$.

Since the orthorhombic $MAPbI_3$ is a direct-band-gap crystal,[17,18,30] multiple PL peaks indicate that there are multiple radiative recombination centers involved, *e.g.*, intrinsic defect states, extrinsic impurities, and residual tetragonal $MAPbI_3$ crystals.

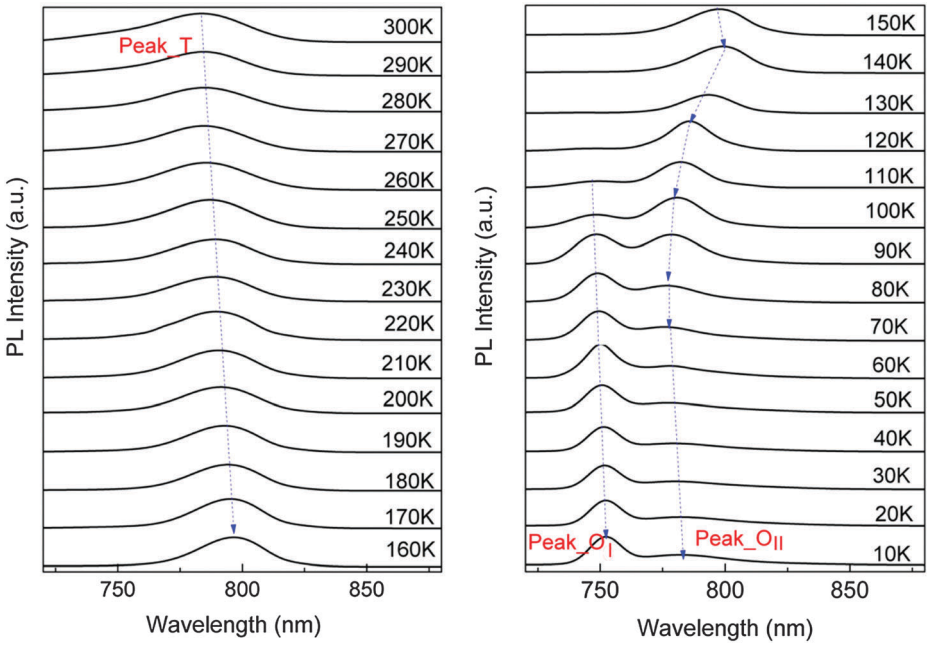

Fig. 2 PL spectra of the $MAPbI_3$ perovskite-crystal film at variable temperatures, the arrows indicate the evolution of the maximum of the PL band: (a) $MAPbI_3$ in the tetragonal phase and (b) $MAPbI_3$ in the orthorhombic phase.

As mentioned in the Introduction, there are two different viewpoints on the origin of Peak_O_{II}: (1) the inclusion of the tetragonal phase[11,13] and (2) bound-state excitons in orthorhombic $MAPbI_3$.[12] However, the origin of the continuous variations in PL resulting from the phase transition was disregarded. In order to solve this problem, TRPL is performed at three typical temperatures around the phase transition temperature, ranging from 150 to 100 K. Fig. 3(a–c) shows TRPL spectra of the $MAPbI_3$ perovskite at different time delays after the excitation pulse, where the dashed lines denote the shift of the emission peaks. The TRPL spectra of $MAPbI_3$ measured at high temperatures are also provided in Fig. S2 (ESI†) for comparison. As shown in Fig. S2 (ESI†), there are no obvious emission energy shifts with time delay after excitation in tetragonal $MAPbI_3$. This observation is consistent with previous reports on the homogeneously broadened emission line width of tetragonal $MAPbI_3$.[8,24] By contrast, at 140 K, Peak_O_{II} slightly red-shifts with time after excitation, indicating a different emission mechanism from that of Peak_T. As T further decreases, a more evident red-shift in Peak_O_{II} is observed. This observation suggests that there is a migration of photo-excited carriers to lower energy sites as a function of time delay after a pulsed excitation. The evident temporal red shift in Peak_O_{II} at 120 K coincides well with a DAP recombination behavior. The photon energy and the recombination rate of the DAP-related emission are determined by the following equations, respectively:

$$\hbar\omega = E_g - E_A - E_D + e^2/(4\pi\varepsilon_0\varepsilon R) \quad (1)$$

$$1/\tau_{DA} \propto \exp[-2(R/\alpha_{D,A})] \quad (2)$$

where E_g is the band-gap energy, ε_0 is the static dielectric constant and E_D and E_A are the donor and acceptor binding energies, respectively; R is the distance between ionized donors and acceptors; $(\tau_{DA})^{-1}$ and $\alpha_{D,A}$ are the radiative recombination rate and the larger Bohr-radius equivalent of the donor and acceptor, respectively. Thus, the emission energy ($\hbar\omega$) from the spatially close pairs is higher than that from the spatially distant pairs because of the larger Coulomb interactions for the former. In addition, the electron–hole recombination probability for close pairs is higher than that for distant pairs because of greater wave function overlap. Therefore, the recombination rate for the high-energy transition is larger than that for the low-energy transition, which results in faster decay times for the photons with shorter wavelengths in the PL band.[32] The wavelength-dependent PL lifetimes measured at different T are illustrated in Fig. 3(d). The lifetimes are obtained by fitting tri-exponential decay functions. The difference between the lifetimes on the long and short wavelength sides is gradually increased from <50 ns at 140 K to 270 ns at 120 K. We thus conclude that Peak_O_{II} is due to the DAP recombination at $T < 120$ K. As T is in the range of 140 to 120 K, $MAPbI_3$ is in a transition state where two phases coexist. The TRPL spectra demonstrate that the transition from Peak_T (NBE recombination) to Peak_O_{II} (DAP recombination) is a gradual process. The gradually increased red shift in Peak_O_{II} with a decrease in T can be interpreted as the decreased content of the tetragonal inclusions in the host orthorhombic $MAPbI_3$. Herein, we propose that Peak_O_I is the NBE emission of the orthorhombic $MAPbI_3$, *i.e.*, free exciton recombination due to the large binding energy at low temperature range as discussed above. This can be explained as follows: on the one side, the emission energy of Peak_O_I locates at 740–750 nm (as shown in Fig. 2(b)), which is close to the absorption maximum of orthorhombic $MAPbI_3$ (740–760 nm).[31] On the other side, after a pulsed excitation, no time-dependent emission-energy shift

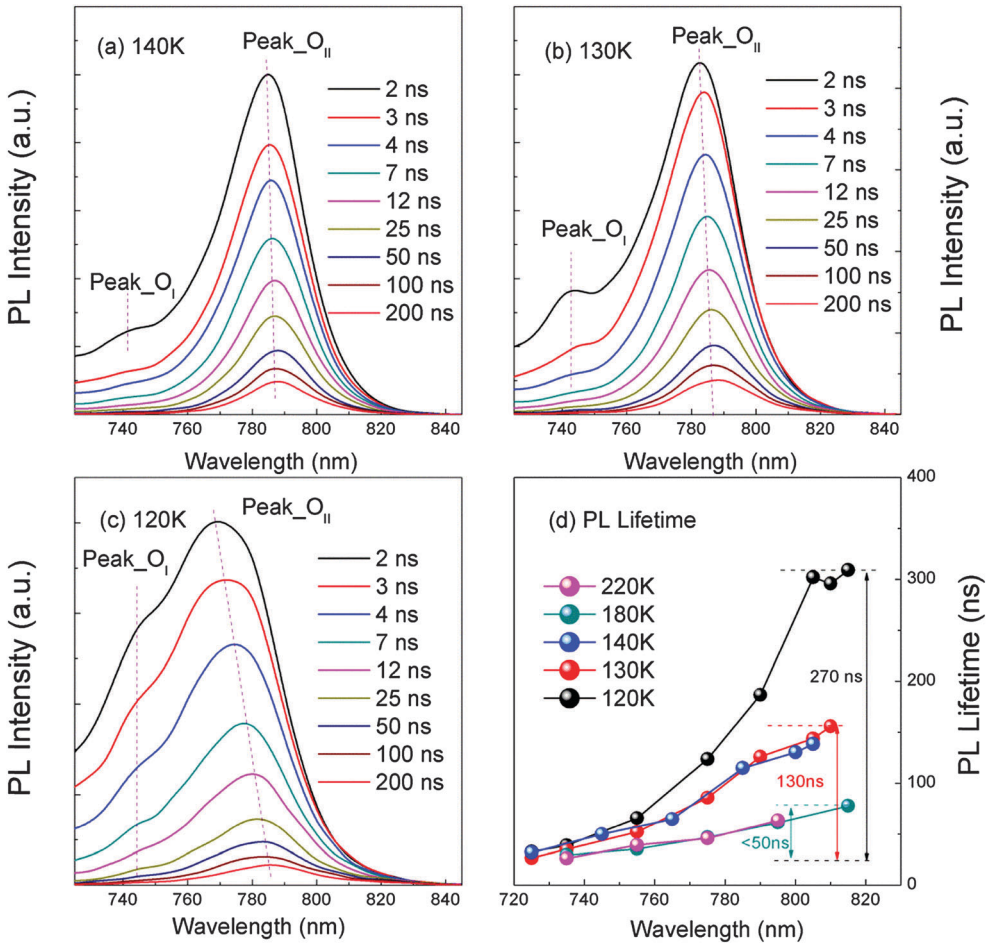

Fig. 3 TRPL spectra of $MAPbI_3$ measured at (a) 140 K, (b) 130 K, and (c) 120 K. (d) Wavelength dependent PL lifetimes of $MAPbI_3$ at different temperatures.

can be observed, which is similar to the case of Peak_T in tetragonal $MAPbI_3$.

Tetragonal inclusions in the orthorhombic phase of $MAPbI_3$ can potentially trap photo-excited excitons due to the narrower band gap of tetragonal $MAPbI_3$ crystals than orthorhombic.[18,33] Thus, a large density of free excitons could agglomerate and eventually recombine within these inclusions.[12] This proposal can be supported by the fast quenching (within less than 10 nanoseconds) of Peak_O_I at 120 and 130 K as shown in Fig. 3(a and b). It can additionally explain the blue-shift in Peak_O_{II} with a decrease in T beginning from 140 K rather than from 160 K. Particularly, the excitons with a large binding energy trapped in tetragonal $MAPbI_3$ during phase transition provides a potential candidate for optoelectronic device applications, especially for lasers since the exciton confinement can lower down the gain threshold.[7] Fig. 4 illustrates the physical picture of the carrier transfer and recombination processes in the coexisting phases.

Since Peak_O_{II} begins to red-shift when T is lower than $\sim$80 K, as shown in Fig. 2(b), the PL properties of the orthorhombic $MAPbI_3$ in the temperature range $<$80 K are further studied by performing an additional excitation-power-dependent PL measurement at 77 K. The results are shown in Fig. 5. Due to the limited

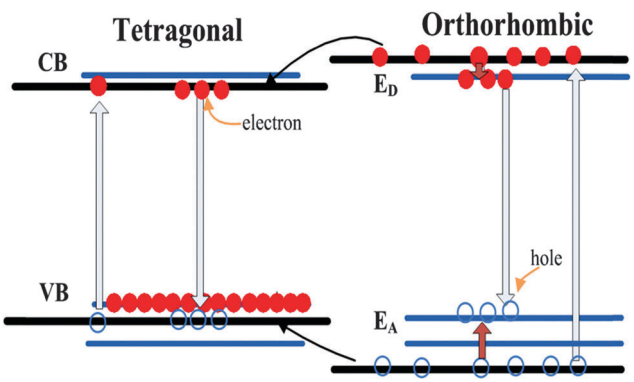

Fig. 4 Diagrams schematically displaying the band structure for the two phases of the $MAPbI_3$ perovskite at 130–150 K. Excitons are confined in the tetragonal phase due to the narrower band gap of the tetragonal $MAPbI_3$.

density of defect states in the crystal, the emission intensity of Peak_O_{II} exhibits a clear saturation behavior at high excitation powers, as shown in the inset of Fig. 5, whereas the emission intensity of Peak_O_I increases almost linearly with increasing excitation power. This fact manifests the free-exciton nature of the emission labeled Peak_O_I, while Peak_O_{II} denotes the emission related to defect states in the crystals, *i.e.* DAP related transition.

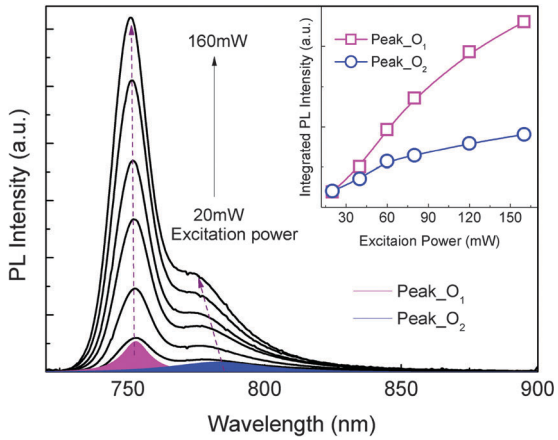

Fig. 5 The excitation power dependent PL spectra of $MAPbI_3$ measured at 77 K. Peak_O_I and O_{II} are obtained by Lorentzian deconvolution from the PL spectra of $MAPbI_3$ which are highlighted with pink and blue, respectively. Inset: the evolution of the PL intensity for Peak_$O_{I,II}$ along with increasing excitation power.

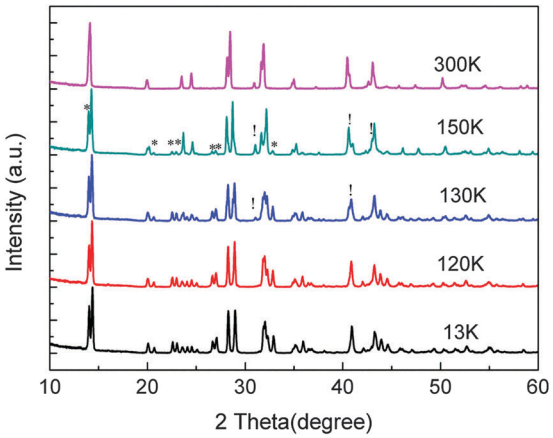

Fig. 6 (a) XRD patterns of $MAPbI_3$ at typical temperatures. The exclamatory marks and asterisks are used to identify the existence of tetragonal and orthorhombic phases, respectively.

Besides, as the excitation power increases from 20 to 160 mW, Peak_O_{II} blue-shifts from 783 to 777 nm. This evidence can help one to safely exclude the possibility that Peak_O_{II} originates from free-exciton recombination of the tetragonal $MAPbI_3$, since the blue shift in emission with the increase of the excitation power is a typical characteristic of DAP recombination.[34] At low-power excitation, low density electrons and holes are excited by absorption of the pumping laser beam. The excited carriers can quickly relax to and are trapped by the neutral donors or acceptors, hence primarily distant DAP recombination can occur. While at high-power excitation high density carriers are excited, the relaxation of hot carriers leads to the filling up of the donors and acceptor energy levels, thus close DAP recombination can be seen. The DAP-related emission thus blue shifts with the increase of the excitation power according to eqn (1).

Next, we want to support our findings from PL measurements with a complementary investigation of the crystal structure by XRD measurements. Fig. 6 illustrates the XRD patterns of $MAPbI_3$ crystals obtained at different temperatures. At room temperature ($\sim$300 K), the XRD peaks assigned to the (110), (220) and (330) diffraction at 14.109°, 28.461° and 43.062°, respectively, confirm the formation of a tetragonal perovskite structure with lattice parameters of $a = c = 8.866$ Å and $b = 12.668$ Å. At 13 K, strong peaks at 14.359, 28.973, 32.032 and 40.909 Å, corresponding to (101), (202), (301) and (242) diffraction, respectively, confirm the orthorhombic structure of the perovskite with lattice parameters of $a = 8.855$ Å, $b = 12.614$ Å and $c = 8.571$ Å.[1,4,5,35,36] The refined lattice parameters of $MAPbI_3$ at different temperatures ranging from 13 to 300 K are tabulated in Table SI (ESI†). From the XRD pattern at 150 K, which is near the tetragonal–orthorhombic phase transition T,[14,16,33] we can clearly observe the orthorhombic phase (highlighted by asterisks). This observation indicates that there is still a residual tetragonal phase (highlighted by exclamatory marks), although tetragonal–orthorhombic phase transition has already taken place. When T is lower than 130 K, the typical peaks from the tetragonal phase are not observed. Some factors could result in this phase coexistence, such as unequal thermal expansion and the spontaneous change of the in-plane lattice constants during the phase-transition.[12,33] The defects in the $MAPbI_3$ crystal may also induce the phase coexistence.[37,38] Our XRD results clearly show the coexistence of the two phases at T from 150 to 130 K. To the best of our knowledge, this is for the first time that the phase coexistence of $MAPbI_3$ around the tetragonal–orthorhombic phase transition $T_{t\text{-}o}$ is observed through XRD, which has been predicted by previous articles.[11–13,21]

Defects in semiconductors can have an important effect on the optical and electrical properties of the crystals. Without intentional doping, $MAPbI_3$ can perform either as a p or n type conductor, depending on the growth parameters.[17,25,30] This fact confirms the existence of intrinsic defects in the $MAPbI_3$ crystals. Unfortunately, a little literature exists on the defect physics of $MAPbI_3$ around the phase transition T.[15,18,33] Our work shows that donors and acceptors can simultaneously exist in $MAPbI_3$ and their energy levels in the bandgap are temperature dependent. These characters could be utilized in the development of novel optoelectronic devices, for example, one may tune light emission of the material *via* precise control of the operation temperature of a lighting source. The phase transition is primarily induced by the angular distortions of the [PbI6] octahedral, *i.e.*, I^- anions in the c axis direction transversely displace from the mid-point of the Pb–Pb distance to which they are constrained in the ideal crystallographic description.[18,19,33] It is hence expected that if the DAPs are related to I or Pb, the emitting photons by the DAP recombination will give rise to a distinct shift around phase transition $T_{t\text{-}o}$, according to eqn (1). This may explain the blue shift of Peak_ O_{II} as T decreases from 140 to 80 K. Yin *et al.* theoretically predicted the formation energies and the locations of the defects acting as donors and acceptors in the band structure in cubic $MAPbI_3$ perovskite.[30] According to the prediction, lead and iodine vacancies (denoted by V_{Pb}, and V_I, respectively) with low formation energies can be easily formed due to the strong Pb lone-pair s-orbital and I p-orbital antibonding coupling. We thus expect that Peak_O_{II}

observed in orthorhombic $MAPbI_3$ is related to the intrinsic defects, V_{Pb}, and V_I, which needs confirmation by precision calculation of theorists.

4. Conclusions

In this work, we deliberately studied the abnormal luminescence properties of $MAPbI_3$ at the tetragonal–orthorhombic phase transition T ranging from 150 to 120 K. Two luminescence features upon the tetragonal–orthorhombic phase transition are observed in steady-state PL measurements. TRPL, variable-excitation-power PL, and variable-temperature XRD characterization are performed at low temperatures to support the interpretation of the origin of two luminescence features at the phase-transition region of $MAPbI_3$. In conclusion, our PL and XRD results unambiguously reveal the coexistence of the tetragonal and orthorhombic phases of $MAPbI_3$ in the temperature range of 150–130 K. When T is lower than 130 K, the two luminescence features observed in the orthorhombic phase originate from free excitons and DAP transitions, respectively. Our results highlight a comprehensive understanding of optical properties upon phase transition in $MAPbI_3$, and we are confident that the findings will benefit the development of new optoelectronic devices based on perovskite materials.

Acknowledgements

This work was sponsored by National Key Basic Research Program of China (No. 2011CB925603) and National Natural Science Foundation of China (No. 61290305 and 11374259). The authors would like to thank Jinke Bao for variable-temperature XRD measurements.

References

1 H. Zhou, *et al.*, Photovoltaics. Interface engineering of highly efficient perovskite solar cells, *Science*, 2014, **345**(6196), 542–546.
2 G. C. Xing, *et al.*, Long-Range Balanced Electron- and Hole-Transport Lengths in Organic-Inorganic $CH_3NH_3PbI_3$, *Science*, 2013, **342**(6156), 344–347.
3 Z. Ku, *et al.*, Full printable processed mesoscopic CH(3)NH(3)PbI(3)/TiO(2) heterojunction solar cells with carbon counter electrode, *Sci. Rep.*, 2013, **3**, 3132.
4 M. Z. Liu, M. B. Johnston and H. J. Snaith, Efficient planar heterojunction perovskite solar cells by vapour deposition, *Nature*, 2013, **501**(7467), 395–398.
5 J. Burschka, *et al.*, Sequential deposition as a route to high-performance perovskite-sensitized solar cells, *Nature*, 2013, **499**(7458), 316–319.
6 G. E. Eperon, *et al.*, Formamidinium lead trihalide: a broadly tunable perovskite for efficient planar heterojunction solar cells, *Energy Environ. Sci.*, 2014, **7**(3), 982–988.
7 G. C. Xing, *et al.*, Low-temperature solution-processed wavelength-tunable perovskites for lasing, *Nat. Mater.*, 2014, **13**(5), 476–480.
8 C. Wehrenfennig, *et al.*, Homogeneous Emission Line Broadening in the Organo Lead Halide Perovskite $CH_3NH_3PbI_3$–xClx, *J. Phys. Chem. Lett.*, 2014, **5**(8), 1300–1306.
9 F. Deschler, *et al.*, High Photoluminescence Efficiency and Optically Pumped Lasing in Solution-Processed Mixed Halide Perovskite Semiconductors, *J. Phys. Chem. Lett.*, 2014, **5**(8), 1421–1426.
10 T. S. Kao, *et al.*, Lasing behaviors upon phase transition in solution-processed perovskite thin films, *Appl. Phys. Lett.*, 2014, **105**(23), 231108.
11 Y. Yamada, *et al.*, Near-band-edge optical responses of solution-processed organic–inorganic hybrid perovskite $CH_3NH_3PbI_3$ on mesoporous TiO_2 electrodes, *Appl. Phys. Express*, 2014, **7**(3), 032302.
12 C. Wehrenfennig, *et al.*, Charge carrier recombination channels in the low-temperature phase of organic–inorganic lead halide perovskite thin films, *APL Mater.*, 2014, **2**(8), 081513.
13 K. W. Wu, *et al.*, Temperature-dependent excitonic photoluminescence of hybrid organometal halide perovskite films, *Phys. Chem. Chem. Phys.*, 2014, **16**(41), 22476–22481.
14 H.-H. Fang, *et al.*, Photophysics of Organic-Inorganic Hybrid Lead Iodide Perovskite Single Crystals, *Adv. Funct. Mater.*, 2015, **25**(16), 2378–2385.
15 F. Chiarella, *et al.*, Combined experimental and theoretical investigation of optical, structural, and electronic properties of CH(3)NH(3)SnX(3) thin films (X = Cl, Br), *Phys. Rev. B: Condens. Matter Mater. Phys.*, 2008, **77**(4), 045129.
16 Y. Kawamura, H. Mashiyama and K. Hasebe, Structural study on cubic-tetragonal transition of $CH_3NH_3PbI_3$, *J. Phys. Soc. Jpn.*, 2002, **71**(7), 1694–1697.
17 F. Brivio, A. B. Walker and A. Walsh, Structural and electronic properties of hybrid perovskites for high-efficiency thin-film photovoltaics from first-principles, *APL Mater.*, 2013, **1**(4), 042111.
18 Y. Wang, *et al.*, Density functional theory analysis of structural and electronic properties of orthorhombic perovskite $CH_3NH_3PbI_3$, *Phys. Chem. Chem. Phys.*, 2014, **16**(4), 1424–1429.
19 J. Feng and B. Xiao, Crystal Structures, Optical Properties, and Effective Mass Tensors of $CH_3NH_3PbX_3$ (X = I and Br) Phases Predicted from HSE06, *J. Phys. Chem. Lett.*, 2014, **5**(7), 1278–1282.
20 R. Dhanker, *et al.*, Random lasing in organo-lead halide perovskite microcrystal networks, *Appl. Phys. Lett.*, 2014, **105**(15), 151112.
21 T. S. Kao, *et al.*, Lasing behaviors upon phase transition in solution-processed perovskite thin films, *Appl. Phys. Lett.*, 2014, **105**(23), 231108.
22 P. Löper, *et al.*, Complex Refractive Index Spectra of $CH_3NH_3PbI_3$Perovskite Thin Films Determined by Spectroscopic Ellipsometry and Spectrophotometry, *J. Phys. Chem. Lett.*, 2015, **6**(1), 66–71.
23 Y. Yamada, *et al.*, Photoelectronic Responses in Solution-Processed Perovskite $CH_3NH_3PbI_3$ Solar Cells Studied by Photoluminescence and Photoabsorption Spectroscopy, *IEEE Journal of Photovoltaics*, 2015, **5**(1), 401–405.

24 Y. Yamada, *et al.*, Photocarrier Recombination Dynamics in Perovskite $CH_3NH_3PbI_3$ for Solar Cell Applications, *J. Am. Chem. Soc.*, 2014, **136**(33), 11610–11613.
25 C. C. Stoumpos, C. D. Malliakas and M. G. Kanatzidis, Semiconducting Tin and Lead Iodide Perovskites with Organic Cations: Phase Transitions, High Mobilities, and Near-Infrared Photoluminescent Properties, *Inorg. Chem.*, 2013, **52**(15), 9019–9038.
26 H. S. Kim, *et al.*, High Efficiency Solid-State Sensitized Solar Cell-Based on Submicrometer Rutile TiO_2 Nanorod and $CH_3NH_3PbI_3$ Perovskite Sensitizer, *Nano Lett.*, 2013, **13**(6), 2412–2417.
27 T. Supasai, *et al.*, Formation of a passivating $CH_3NH_3PbI_3$/PbI_2 interface during moderate heating of $CH_3NH_3PbI_3$ layers, *Appl. Phys. Lett.*, 2013, **103**(18), 183906.
28 M. Xu, *et al.*, Highly ordered mesoporous carbon for mesoscopic $CH_3NH_3PbI_3/TiO_2$ heterojunction solar cell, *J. Mater. Chem. A*, 2014, **2**(23), 8607–8611.
29 A. Yella, *et al.*, Nanocrystalline Rutile Electron Extraction Layer Enables Low-Temperature Solution Processed Perovskite Photovoltaics with 13.7% Efficiency, *Nano Lett.*, 2014, **14**(5), 2591–2596.
30 W.-J. Yin, T. Shi and Y. Yan, Unusual defect physics in $CH_3NH_3PbI_3$ perovskite solar cell absorber, *Appl. Phys. Lett.*, 2014, **104**(6), 063903.
31 V. D'Innocenzo, *et al.*, Excitons versus free charges in organo-lead tri-halide perovskites, *Nat. Commun.*, 2014, **5**, 3586.
32 Y. Hamanaka, *et al.*, Photoluminescence Properties and Its Origin of AgInS2Quantum Dots with Chalcopyrite Structure, *J. Phys. Chem. C*, 2011, **115**(5), 1786–1792.
33 T. Baikie, *et al.*, Synthesis and crystal chemistry of the hybrid perovskite $(CH_3NH_3)PbI_3$ for solid-state sensitised solar cell applications, *J. Mater. Chem. A*, 2013, **1**(18), 5628–5641.
34 Y. Hamanaka, *et al.*, Luminescence properties of chalcopyrite AgInS2 nanocrystals: Their origin and related electronic states, *J. Lumin.*, 2013, **133**, 121–124.
35 J. H. Heo, *et al.*, Efficient inorganic–organic hybrid heterojunction solar cells containing perovskite compound and polymeric hole conductors, *Nat. Photonics*, 2013, **7**(6), 486–491.
36 J. Y. Jeng, *et al.*, $CH_3NH_3PbI_3$ Perovskite/Fullerene Planar-Heterojunction Hybrid Solar Cells, *Adv. Mater.*, 2013, **25**(27), 3727–3732.
37 X. B. Chen, *et al.*, Raman analyses of co-phasing and hysteresis behaviors in V_2O_3 thin film, *J. Raman Spectrosc.*, 2012, **43**(12), 2025–2028.
38 P. J. Schilling, *et al.*, Two-phase coexistence region in mechanically alloyed Cu-Fe: An X-ray absorption near-edge structure study, *Acta Mater.*, 1999, **47**(8), 2525–2537.